Journal of Sound and Vibration (2000) **238**(3), 495–527
doi:10.1006/jsvi.2000.3208, available online at http://www.idealibrary.com on IDEAL®

AN EFFICIENT CRANKSHAFT DYNAMIC ANALYSIS USING SUBSTRUCTURING WITH RITZ VECTORS

Z. P. MOURELATOS

Vehicle Analysis & Dynamics Lab, GM Research & Development and Planning, Mail Code 480-106-256, 30500 *Mound Rd, Warren, MI* 48090-9055, *U.S.A. E-mail: zissimos_p._mourelatos@notes.gmr.com*

(*Received* 2 *August* 1999, *and in final form* 3 *July* 2000)

A structural analysis using dynamic substructuring with Ritz vectors is presented for predicting the dynamic response of an engine crankshaft, based on the finite-element method. A two-level dynamic substructuring is performed using a set of load-dependent Ritz vectors. The rotating crankshaft is properly coupled with the non-rotating, compliant engine block. The block compliance is represented by a distributed linear elastic foundation at each main bearing location. The stiffness of the elastic foundation can be different in the vertical and horizontal planes, thereby considering the anisotropy of the engine block compliance with respect to the crankshaft rotation. The analysis accounts for the kinematic non-linearity resulting from the crankangle-dependent circumferential contact location between each journal and the corresponding bore of the engine block. Crankshaft "bent" and block "misboring" effects due to manufacturing imperfections are considered in the analysis. The superior accuracy and reduced computational effort of the present method as compared with the equivalent superelement analysis in MSC/NASTRAN, are demonstrated using the free and forced vibrations of a slender cylindrical beam and free vibrations of a four-cylinder engine crankshaft. Subsequently, the accuracy of the present method in calculating the dynamic response of engine crankshafts is shown through comparisons between the analytical predictions and experimental results for the torsional vibrations of an in-line five cylinder engine and the bending vibrations of the crankshaft-flywheel assembly of a V6 engine.

1. INTRODUCTION

Legislative and customer pressures on engine design call for maximization of engine power, minimization of engine size and improvement of fuel economy, simultaneously. This requires optimized engine components, if competitive designs must be realized. Therefore, sophisticated tools are needed to analyze engine components. This is particularly true of crankshafts, one of the most analyzed engine components.

Many sophisticated crankshaft analysis methods have been reported in the past years. This has been facilitated mostly by the use of the finite-element method on high-speed computers and the availability of elaborate finite-element preprocessors which can construct complex finite-element models. For engine crankshafts, sophisticated analyses have been mainly used in two areas. First, in accurate prediction of crankshaft fillet stresses [1–3], and second in free and forced vibration analysis tailored towards engine noise predictions [4–13].

To analyze the engine crankshaft, a system model of the whole engine must be used. Such a system consists of the crankshaft and the engine block coupled by the hydrodynamically

0022-460X/00/480495 + 33 $35.00/0

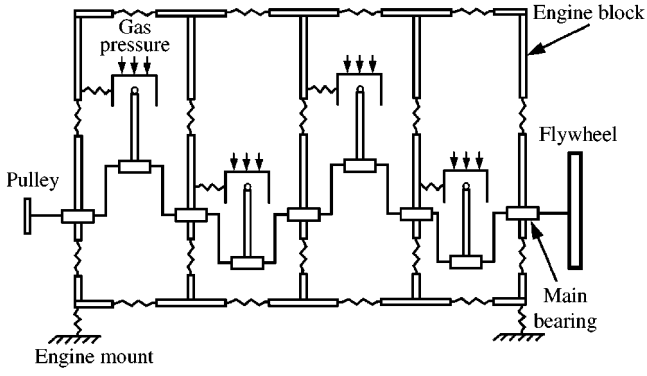

Figure 1. Schematic of the crankshaft—engine block system.

lubricated main bearings (see Figure 1). The loading on the system comes from the cylinder pressure and the piston-connecting rod inertia. The cylinder pressure applied on the piston crown is transmitted to the crankpin through the piston-connecting rod assembly. The inertia of the piston-connecting rod provides a load on the crankpin as well. The crankpin loads deform the crankshaft structure and are transmitted to the engine block at the main bearing locations through the main bearing hydrodynamics. Both the deformation of the crankshaft and engine block affect the main bearing film thickness and therefore, the bearing hydrodynamics. For this reason, the mathematical modelling of the described engine system requires three individual submodels which are coupled together. First, a structural model of the crankshaft, second a structural model of the engine block, and third a lubrication model of the main bearings.

This work describes a finite-element based dynamic crankshaft-engine block structural model using dynamic substructuring with Ritz vectors. It couples the crankshaft model with the engine block flexibility accounting for the crankshaft rotation as seen by the fixed in space engine block. The engine block flexibility is represented by linear springs at the main bearing locations accounting for the block static (not dynamic) stiffness. It has been observed, from extensive application of the present work in crankshaft analysis studies, that the use of the static block stiffness, instead of the dynamic stiffness, can give very good results for a variety of crankshaft studies of practical importance. Some of these studies are presented in Sections 6.3 and 6.4. The block dynamic stiffness however, is ultimately needed for detailed bearing cup stress analysis and noise and vibration studies of the lower engine block. Although not presented in this paper, the present crankshaft-engine block model can be also coupled with a main bearing hydrodynamics model to provide a complete engine crankshaft system model.

Previous crankshaft analyses are either static [1], or use a beam representation of the crankshaft [4, 5]. In an attempt to improve the accuracy, static crankshaft analysis with a correction for the flywheel dynamic behavior was used in references [6, 7]. However, all analyses in references [1, 4–7] fail to represent the crankshaft dynamic behavior, which can be very important under certain operating conditions or even essential for noise and vibration analysis of a crankshaft-engine block system. The idea of using dynamic substructuring in crankshaft analysis has been introduced in references [8, 9]. The MSC/NASTRAN superelement capability [14] was used to perform a dynamic analysis of a long stroke diesel engine crankshaft using component mode synthesis. The modal matrix, composed of the first few crankshaft eigenvectors, was used as the transformation basis. The present analysis does not rely on any of the simplifying assumptions of references

[1, 4–7]. Furthermore, it can be even more accurate and computationally more efficient than the analysis of references [8, 9] since it uses Ritz vectors instead of eigenvectors to form the transformation basis. Ritz vectors are easier to compute and provide a more accurate dynamic representation of the structure.

The finite-element method has been extensively used in static and dynamic analyses of large structures. Due to the structural complexity of the crankshaft, a model with 20 000–30 000 degrees of freedom is common. Although a static analysis of such a model can be easily performed, a dynamic analysis may be impractical due to limitations in computer storage, computing time and cost. To overcome this difficulty, transfer matrix approaches [13] or dynamic substructuring [14] have been proposed in the literature. A dynamic substructuring analysis using special Ritz vectors is used in this work. In a dynamic substructuring analysis, the structure is divided into parts, which are analyzed independently and subsequently, synthesized in order to determine the response of the whole structure. This is similar to conventional modal synthesis techniques [15] using eigenvectors.

A two-level dynamic substructuring analysis, using Ritz vectors, which can accurately predict the dynamic behavior of an engine crankshaft with minimal computational effort, is described here. A representation of the engine block flexibility is given and the combined crankshaft-engine block structural model is formulated. The superior accuracy and reduced computational effort of the present method as compared with the equivalent superelement analysis in MSC/NASTRAN [4, 16], are demonstrated using the free and forced vibrations of a slender cylindrical beam and free vibrations of a four-cylinder engine crankshaft. Subsequently, the accuracy of the present method in calculating the dynamic response of engine crankshafts is showed through comparisons between the analytical predictions and experimental results for the torsional vibrations of an in-line five-cylinder engine and the bending vibrations of the crankshaft–flywheel assembly of a V6 engine.

The present analysis can also be used to predict crankshaft dynamic stresses, which are essential in assessing durability and fatigue limits of engine crankshafts. It is currently common practice to represent a crankshaft with beams and concentrated masses [13]. The stiffness of the beams and the distribution of masses are commonly chosen so that the first eigenproperties of the beam structure are similar to those of the actual crankshaft. The beam model is subsequently used to calculate the dynamic main bearing reactions, which are then applied back to the three-dimensional crankshaft solid model to obtain the dynamic stresses. This approach is not accurate enough for the following reasons. First, the beam model does not represent the dynamics of the crankshaft correctly since it matches only the first eigenproperties of the actual crankshaft. Second, the beam model cannot represent the damping distribution of the crankshaft, which can greatly affect the magnitude of the dynamic displacements. Furthermore, for correct stress levels, one needs the reaction force distribution (not the concentrated reaction force) around the crankshaft journals. This is especially true for calculations of bearing cap stress levels. The present dynamic substructuring approach addresses all of the above problems. Furthermore, it allows stress calculation only on critical stress areas such as crankshaft fillet regions, without calculating the stress field on the entire crankshaft. This can considerably speed up the computational time allowing crankshaft stress analysis to be performed routinely at the design phase.

The present work represents only the structural part of a computer program named CRANKSYM (Crankshaft System Model). This program can be used to predict the crankshaft dynamic response and main bearing performance considering (1) the crankshaft structural dynamics, (2) the main bearing hydrodynamics and (3) the engine block static flexibility simultaneously, using a system approach.

2. TWO-LEVEL DYNAMIC SUBSTRUCTURING ANALYSIS USING RITZ VECTORS

Dynamic substructuring analysis is commonly used for large complex structures. If the finite-element model of the entire structure consists of a large number of degrees of freedom (d.o.f.), it may be impractical to perform a dynamic analysis based on the finite-element equations of the entire system. There are practical advantages in subdividing the complex crankshaft structure into substructures. If some substructures are identical, substantial savings in computer time can be achieved. Furthermore, if structural modifications are made to one substructure, only that substructure must be modified and therefore, the computational cost of a reanalysis can be significantly reduced. In the developed model, each crankthrow (crankshaft structure between two adjacent main bearings) constitutes a separate substructure. The crankshaft nose and tail (flywheel end) are also treated as separate substructures (see Figure 2).

Due to the structural complexity of the crankshaft, even the analysis of a single substructure is computationally expensive. The computational cost increases even more if the analysis is repeated in a design loop. For this reason, dynamic reduction of the d.o.f. is performed for each crankshaft substructure. A set of very efficiently computed orthonormal Ritz vectors is used as transformation basis. In conventional dynamic reduction methods, the transformation basis consists of the first exact or approximate eigenvectors of the structure (Modal Analysis and Generalized Dynamic Reduction respectively, in MSC/NASTRAN [16]).

The calculation of eigenvectors for a large structure is computationally expensive. Besides, the participation of a particular eigenvector in the final solution depends on the applied dynamic loading. If the loading frequency is close to a natural frequency of the structure, then the corresponding eigenvector participates significantly in the solution. Furthermore, eigenvectors orthogonal to the applied loading do not participate in the solution even if their frequency (corresponding eigenvalue) is contained in the loading. For the above reasons, the eigenvectors may not be the most efficient basis for a dynamic reduction of a complex structure subjected to certain external loading.

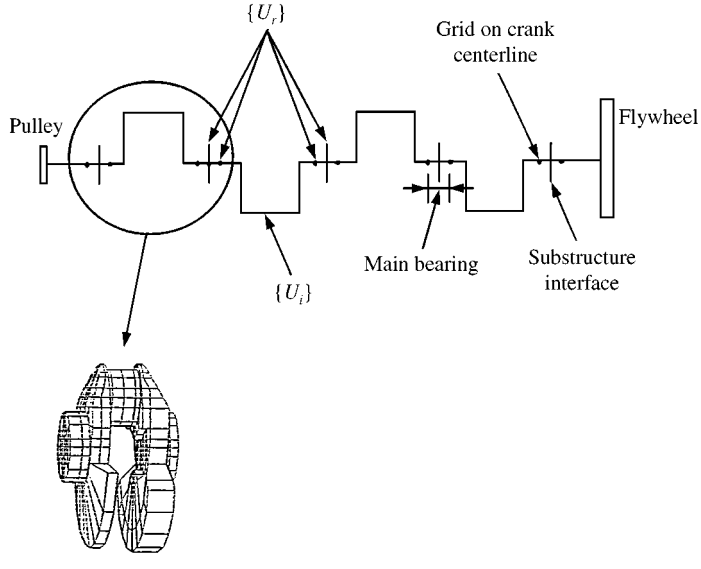

Figure 2. Some definitions on the crankshaft substructuring. $\{U_r\}$: vector of retained d.o.f.; $\{u_i\}$: vector of internal d.o.f.

It has been demonstrated that use of orthonormal Ritz vectors instead of the same number of eigenvectors, can result in better accuracy in dynamic analysis of complex structures [17–22]. The reason is that Ritz vectors consider the spatial distribution of the applied loading, whereas the eigenvectors neglect that important information. The first Ritz vector is the static solution to the applied loading. The subsequent Ritz vectors are generated by multiplying the mass matrix by the previous Ritz vector and use the result as a load vector for a new static solution [17].

2.1. USE OF RITZ VECTORS IN DYNAMIC REDUCTION

The dynamic equilibrium of a structural system modelled using the finite-element method, are written as

$$[M]\{\ddot{U}\} + [C]\{\dot{U}\} + [K]\{U\} = \{F(s, t)\}, \tag{1}$$

where $[M]$, $[C]$, $[K]$ and $\{F\}$ are the mass matrix, damping matrix, stiffness matrix and load vector respectively. The load and displacement (or response) vectors are a function of space (s) and time (t). Equation ((1)) can be solved for the displacement vector $\{U\}$.

If the response vector $\{U\}$ is expressed as

$$\begin{gathered}\{U(s, t)\} = [X(s)]\{u(t)\}, \\ (n \times 1) \qquad (n \times m)\,(m \times 1)\end{gathered} \tag{2}$$

the original equations (1) reduce to

$$[\bar{M}]\{\ddot{u}\} + [\bar{C}]\{\dot{u}\} + [\bar{K}]\{u\} = \{\bar{F}\}, \tag{3}$$

where

$$[\bar{M}] = [X]^{\mathrm{T}}[M][X] \quad (m \times m), \qquad \{\bar{F}\} = [X]^{\mathrm{T}}\{F(s, t)\} \quad (m \times 1). \tag{4}$$

Similar expressions hold for $[\bar{C}]$ and $[\bar{K}]$. In the above equations $[X(s)]$ is a transformation basis matrix and $\{u(t)\}$ is the generalized displacement vector. The dimension m is always much less than n. The dynamic reduction methods are differentiated by the way the transformation basis $[X]$ is formed. MSC/NASTRAN uses the first few exact eigenvectors to form $[X]$ in the modal analysis method and the first approximate eigenvectors in the generalized dynamic reduction method [16]. Superior accuracy and reduced computational effort have been demonstrated with the use of load-dependent Ritz vectors instead of eigenvectors [17–22]. For this reason, Ritz vectors are chosen in this work to form $[X]$.

If the load vector can be represented as the product of one vector of space (s) functions and one time (t) function as

$$\{F(s, t)\} = \{f(s)\}g(t), \tag{5}$$

then the Wilson *et al.* [17] algorithm is a more economical alternative to conventional dynamic reduction techniques which use eigenvectors to form the transformation basis. The Wilson *et al.* algorithm, referred here as single vector Ritz algorithm, uses load-dependent Ritz vectors for the transformation basis. Those vectors are generated by an inverse iteration type of recurrence procedure from the fixed spatial (s) distribution of the dynamic load. The single vector Ritz algorithm has been proven very efficient and accurate for a variety of applications [18–20, 23].

However, for most practical problems, including the crankshaft dynamic response problem, the load vector cannot be expressed as a product of a single space vector and a single time function as in equation (5). Instead, it can be expressed as the superposition of k spatial vectors and k time functions as

$$\{F(s, t)\} = \sum_{i=1}^{k} \{f_i(s)\}\{g_i(t)\}. \tag{6}$$

In such a case, the single vector Ritz algorithm can be used only if k different reduced subsystems are formed and solved independently. For the ith subsystem, a transformation basis is generated corresponding to the ith spatial load vector $f_i(s)$. If the original system is linear, its solution is the superposition of all the subsystem solutions.

This approach can be very inefficient since k different subsystems are solved independently. Furthermore, if the dynamic substructuring is used, the solution of each subsystem may be inaccurate. In dynamic substructuring, each subsystem will have only one loaded substructure. The transformation basis for each substructure exists only for the loaded substructure since it is based on load-dependent Ritz vectors. Although the loaded substructure will be accurately reduced, the unloaded substructures will be reduced by Guyan reduction [17, 24] which may be inaccurate. This point will be fully illustrated in the next section.

For the above reasons, if there is a multispatial load on the structure described by equation (6), the single vector Ritz algorithm may be inefficient and more importantly inaccurate in dynamic substructuring calculations. In this work, a load-dependent subspace reduction method which is a modification of the methods presented in references [21, 25] is used. It is an extension of the single vector Ritz algorithm and eliminates the described deficiencies of the single vector Ritz algorithm in dynamic substructuring. The transformation basis consists of load-dependent vectors generated by a recurrence sequence which uses blocks of vectors corresponding to the multiload spatial vectors of the initial system. The method is described in Appendix A.

The initial block of vectors $[X^*]$ corresponding to the static deflection of the structure subjected to the specified multiload spatial vectors $[F]$ is first generated (step 3a) and all vectors in $[X^*]$ are M-normalized (step 3b) to form block $[X]$. Subsequently, the vectors in $[X]$ are M-orthogonalized using Gram–Schmidt orthogonalization to remove common components in the transformation basis (step 3c) and M-normalized again (step 3d). The M-normalization of step 3b was found necessary for the M-orthogonalization of the next step to produce M-orthogonal vectors. The recurrence procedure of step 4 is used to generate additional blocks of Ritz vectors. A block of vectors $[X_i^*]$ representing the static response of the structure subjected to an updated static vector block is found (step 4a). The block $[X_i^*]$ is subsequently M-orthogonalized twice against all previous blocks (steps 4b and c) to form $[X_i]$. Finally, all vectors in $[X_i]$ are M-orthonormalized (step 4d) and added to the transformation basis. Double orthogonalization was found necessary because single orthogonalization fails to produce orthogonal blocks of vectors after the first few steps. Double orthogonalization is also used during the generation of approximate eigenvectors for the generalized dynamic reduction method in MSC/NASTRAN [16].

The proposed subspace reduction method is more efficient compared with the classical subspace or Lanczos eigensolvers since no iteration on the reduced eigenproblem needs to be performed, no convergence test is performed for the computed Ritz vectors and no Sturm sequence is required to verify the acceptance of computed eigenvectors as is normally done for the Lanczos method [16, 26].

The efficiency and accuracy of the present subspace reduction method depends on the number of independent spatial load vectors k in block $[F]$ and the number of blocks of Ritz vectors, or steps in the algorithm, p. The number of orthonormal Ritz vectors $m = k * p$ in the final transformation basis determines the dimension of the reduced dynamic system of equation (3). For computational efficiency, m should be as small as possible without jeopardizing the accuracy of the reduced system. If k is large, then p should be kept small which may lead to poor approximation of the dynamic effects and consequently poor accuracy. Therefore, k should be as small as possible.

In the present dynamic substructuring analysis of engine crankshaft structures, the crankshaft segment between two adjacent main bearings constitutes a substructure. The external load on each substructure is applied on each crankpin. For in-line engine configurations there is only one crankpin per substructure while for V-engine configurations there are two crankpins per substructure. The load on each crankpin is decomposed into a vertical and a horizontal component. Therefore, k is equal to two for in-line engines and equal to four for V-engines. Since it is not necessary to use all the independent spatial vectors [25], only one vertical and one horizontal spatial vector for each substructure are used in the present work for both in-line and V-engines. This reduces k to two.

2.2. FIRST LEVEL OF DYNAMIC SUBSTRUCTURING ANALYSIS

The crankshaft is divided into a number of substructures by splitting it at the middle of each main bearing location. The initial displacement vector $\{U\}$ of equation (1) is partitioned into internal displacements $\{U_i\}$ and retained displacements $\{U_r\}$. The vector $\{U_r\}$ consists of all the displacements of the common interfaces of the substructures plus the displacements of points on the crankshaft centerline at the two ends of each main bearing (see Figure 2). The latter points are used to determine the slope of each main bearing journal. $\{U_i\}$ includes all other displacements in $\{U\}$. Based on this partitioning, the initial displacement vector $\{U\}$, load vector $\{F\}$ and the mass matrix in equations (1) are rewritten as

$$\{U\} = \{U_i^1 \; U_i^2 \ldots | U_r\}^{\mathrm{T}}, \quad \{F\} = \{F_i^1 \; F_i^2 \ldots | F_r\}^{\mathrm{T}}, \tag{7, 8}$$

$$[M] = \left[\begin{array}{c|c} M_i & M_{ir} \\ \hline M_{ir}^{\mathrm{T}} & M_i \end{array}\right] = \begin{bmatrix} M_i^1 & 0 & \cdots & M_{ir}^1 \\ 0 & M_i^2 & \cdots & M_{ir}^2 \\ \vdots & & \ddots & \\ M_{ir}^{1\mathrm{T}} & M_{ir}^{2\mathrm{T}} & \cdots & M_r \end{bmatrix}. \tag{9}$$

Similar expressions hold for C and K matrices. In equations (9), the zeros represent null matrices of the appropriate dimensions. Subscripts i and r denote internal and retained degrees of freedom, respectively, and superscripts denote the substructure number or the transpose of a matrix. Each crankthrow (crank bay) and the crankshaft nose and tail constitute separate substructures.

According to equation (2), the internal displacement vector $\{U_i^\ell\}$ for the ℓth substructure is transformed as

$$\{U_i^\ell\} = [X^\ell]\{u^\ell\}. \tag{10}$$

The transformation matrix $[X^\ell]$ consists of a set of M-orthonormal Ritz vectors calculated with the algorithm of Appendix A based on matrices $[M_i^\ell]$, $[K_i^\ell]$ and $[F_i^\ell]$ for the ℓth substructure. Matrix $[F_i^\ell]$ consists of only two spatial load vectors ($k = 2$). For in-line engines, they are the vertical and horizontal spatial loads on the single crankpin. For V-engines, they are the vertical spatial load on one crankpin and the horizontal spatial load on the second crankpin.

By using matrices $[M_i]$, $[K_i]$ and $[F_i]$ in the calculation of $[X]$, the retained d.o.f $\{U_r\}$ are assumed equal to zero. This is similar to calculating fixed-interface modes in the traditional Craig–Bampton method [27]. However, $\{U_r\}$ is not zero and therefore, results in additional internal displacements $\{U_i^\ell\}$ which are assumed to satisfy the static relationship

$$[K_i^\ell]\{U_i^\ell\} + [K_{ir}^\ell]\{U_r\} = 0 \tag{11a}$$

from which we get

$$\{U_i^\ell\} = -[K_i^\ell]^{-1}[K_{ir}^\ell]\{U_r\} = [T^\ell]\{U_r\}, \tag{11b}$$

where

$$[T^\ell] = -[K_i^\ell]^{-1}[K_{ir}^\ell] \tag{12}$$

is the static transformation matrix between $\{U_i^\ell\}$ and $\{U_r\}$. If equations (10) and (11) are grouped together for all substructures, we get

$$\{U\} = \begin{bmatrix} U_i^1 \\ \vdots \\ U_i^\ell \\ \vdots \\ \hline U_r \end{bmatrix} = \left[\begin{array}{cccc|c} X^1 & \cdots & 0 & \cdots & T^1 \\ \vdots & & \vdots & & \vdots \\ 0 & \cdots & X^l & \cdots & T^\ell \\ \vdots & & \vdots & & \vdots \\ \hline 0 & \cdots & 0 & \cdots & I \end{array}\right] \begin{bmatrix} u^1 \\ \vdots \\ u^\ell \\ \vdots \\ \hline U_r \end{bmatrix} = [\Phi]\{\bar{u}\}. \tag{13}$$

Substitution of equation (13) in the partitioned equation (1) and premultiplication with $[\Phi]^{\mathrm{T}}$ yields

$$[\bar{M}]\{\ddot{\bar{u}}\} + [\bar{C}]\{\dot{\bar{u}}\} + [\bar{K}]\{\bar{u}\} = \{\bar{F}\}, \tag{14}$$

where

$$[\bar{M}] = [\Phi]^{\mathrm{T}}[M][\Phi] = \begin{bmatrix} \bar{M}_i^1 & \cdots & 0 & \cdots & \bar{M}_{ir}^1 \\ \vdots & & \vdots & & \vdots \\ 0 & \cdots & \bar{M}_i^\ell & \cdots & \bar{M}_{ir}^\ell \\ \vdots & & \vdots & & \vdots \\ \bar{M}_{ir}^{1T} & \cdots & \bar{M}_{ir}^{\ell T} & \cdots & \bar{M}_r \end{bmatrix}, \tag{15}$$

$$\bar{M}_i^\ell = X^{\ell T} M_i^\ell X^\ell, \quad \bar{M}_{ir}^\ell = X^{\ell T}(M_i^\ell T^\ell + M_{ir}^\ell), \tag{15a, b}$$

$$\bar{M}_r = M_r + \sum_\ell (T^{\ell T} M_i^\ell T^\ell + M_{ir}^{\ell T} T^\ell + T^{\ell T} M_{ir}^\ell). \tag{15c}$$

Similar expressions hold for $\bar{C}$ and $\bar{K}$. The reduced load vector $\{\bar{F}\}$ is given by

$$\{\bar{F}\} = \{\bar{F}_i^1 \cdots \bar{F}_i^\ell \cdots \bar{F}_r\}^{\mathrm{T}}, \tag{16}$$

where

$$\bar{F}_i^\ell = X^{\ell} F_i^\ell, \quad \bar{F}_r = F_r + \sum_\ell T^{\ell} F_i^\ell. \tag{16a, b}$$

Since the Ritz vectors are M-orthonormalized,

$$\bar{M}_i^\ell = X^{\ell T} M_i^\ell X^\ell = I. \tag{17}$$

Furthermore, due to equation (11),

$$\bar{K}_{ir}^\ell = X^{\ell T}(K_i^\ell T^\ell + K_{ir}^\ell) = 0. \tag{18}$$

If the number of Ritz vectors, or equivalently the number of generalized coordinates u, is zero for every substructure, equation (13) reduces to

$$[\bar{M}_r]\{\ddot{U}_r\} + [\bar{C}_r]\{\dot{U}_r\} + [\bar{K}_r]\{U_r\} = \{\bar{F}_r\}, \tag{19}$$

which is the Guyan dynamic reduction technique. The Guyan reduction is exact for static loading. However, depending on the selection of the retained d.o.f., it can be inaccurate for dynamic analysis [16].

2.3. SECOND LEVEL OF DYNAMIC SUBSTRUCTURING ANALYSIS

In the first level of substructuring analysis, equation (14) is solved for the reduced displacement vector

$$\{\bar{u}\} = \{u^1 \;\; u^2 \;\; \ldots \;\; u^\ell \;\; \ldots \,|\, U_r\}^{\mathrm{T}}, \tag{20}$$

where u^ℓ is the generalized displacement vector of the ℓth substructure and $\{U_r\}$ is the vector of the retained displacements. Recall that $\{U_r\}$ contains all the displacements of the common interfaces of the substructures plus the displacements of points on the crankshaft centerline at the two ends of each main bearing (see Figure 2). Even for a coarse finite-element mesh of the crankshaft, the number of the retained displacements for the substructure interfaces can be fairly large. For this reason, a second level of substructuring is performed which further reduces the number of retained degrees of freedom.

For the second level of substructure analysis, $\{U_r\}$ is partitioned as

$$\{{}_1U_r\} = \{{}_2U_i \;\; {}_2U_r\}^{\mathrm{T}}, \tag{21}$$

where the left subscript indicates the level of substructuring analysis. $\{{}_2U_r\}$ contains the displacements of three points at the left end, middle and right end of each main bearing on the crankshaft centerline. $\{{}_2U_i\}$ includes all the other displacements of the substructure interfaces which were retained in the first level of substructuring. Due to the partitioning of equation (21), equation (20) becomes

$$\{{}_1\bar{u}\} = \{{}_2u_i \;\; {}_2U_r\}^{\mathrm{T}}, \tag{22a}$$

where

$$\{{}_2u_i\} = \{{}_1u^1 \;\; \ldots \;\; {}_1u^\ell \;\; \ldots \;\; {}_2U_i\}^{\mathrm{T}}. \tag{22b}$$

The reduced matrices $[\bar{M}], [\bar{C}]$ and $[\bar{K}]$ and the load vector $\{\bar{F}\}$ from the first level of substructuring are partitioned according to equation (22), and the process described in the previous paragraph is repeated. A new Ritz transformation matrix $[X]$ is calculated using again the algorithm of Appendix A, and a new reduced system, similar to that of equation (14), is formed.

3. IMPLEMENTATION OF THE DYNAMIC SUBSTRUCTURE ANALYSIS

The previously described two-level dynamic substructure analysis and the algorithm to find the Ritz vectors (see Appendix A) can be easily coded into a FORTRAN code. However, there is a serious problem with data management. The original crankshaft finite-element model commonly consists of more than 20 000 d.o.f. The stiffness, mass and damping matrices as well as a variety of other auxiliary large matrices cannot be stored in core computer memory due to computer storage limitations. For this reason, the data management capabilities of the general purpose code MSC/NASTRAN [16, 26] are used.

Initially, MSC/NASTRAN calculates the mass and stiffness matrices of the model. Then two separate DMAP ALTERS [28], instruct MSC/NASTRAN to implement the Ritz vector algorithm of Appendix A for the two levels of substructuring. An MSC/NASTRAN job for each substructure is submitted to perform the first level of dynamic substructuring calculations. MSC/NASTRAN calculates and stores internally the stiffness and mass matrices of the original substructure models. Then it implements the algorithm to find the first level Ritz vectors and also calculates and stores the reduced matrices of equation (14) in separate files for each substructure. After the first level of calculations has been completed, another MSC/NASTRAN job is submitted for the second level of substructuring. MSC/NASTRAN first reads the first-level reduced matrices and then assembles all the substructures. Subsequently, it partitions the first level reduced displacement vector according to equation (22) and finds the second-level Ritz vectors. Finally, it calculates the final reduced stiffness and mass matrices for the whole crankshaft and stores the results in a file. These are subsequently read by a FORTRAN code, which performs the time integration of the reduced model.

After the two reductions, the reduced model consists of approximately 50–100 d.o.f. only. This translates to substantial computational savings in performing a crankshaft dynamic analysis. The computational savings become even more important when the crankshaft dynamic analysis is coupled with the main bearing hydrodynamics to calculate the combined system response.

4. ENGINE BLOCK STIFFNESS

The reduced crankshaft model, as described in the previous paragraphs, is supported at the main bearing locations. The support is provided by the engine block. The engine block stiffness can be represented by a vertical and horizontal value for each main bearing. In practice, the vertical and horizontal stiffnesses are always different. The vertical stiffness can be an order of magnitude larger than the horizontal stiffness. Besides, both the vertical and the horizontal stiffnesses vary around the circumference of each main bearing.

The engine block support can be modelled by a concentrated stiffness at the midbearing position or by a distributed stiffness along the bearing length. In the former case, the bearing loads consist of reaction forces only. If these loads are used in a traditional main bearing lubrication analysis, there will be no journal misalignment. However, dynamic

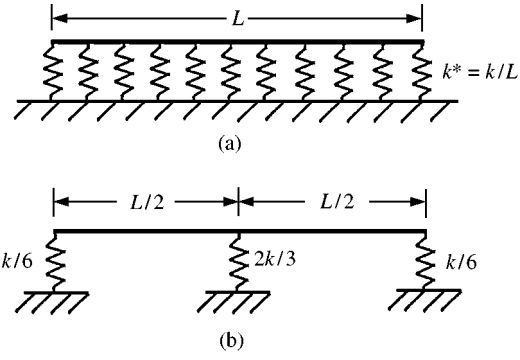

Figure 3. Representation of the engine block stiffness. (a) Distributed engine block stiffness, (b) equivalent distributed engine block stiffness.

misalignment can have a significant influence on the main bearing performance. The issue of dynamic misalignment can be of concern with the increasing number of four-cylinder engines and V6 configurations where adequate main bearing performance remains a design challenge.

The journal misalignment can be calculated by modelling the engine block flexibility with a distributed stiffness along the bearing length (see Figure 3(a)). In this study, three linear springs are used along the bearing length (one spring at each bearing end and one spring at the midbearing location) to represent the distributed engine block flexibility in both the vertical and horizontal planes (see Figure 3(b)). This representation accounts for the translational and rotational engine block stiffness. As a result, the bearing loads consist of reaction forces and reaction moments. If the translational bearing stiffness is k, the three springs have stiffnesses $k/6$, $2k/3$ and $k/6$ (see Figure 3(b)). These stiffnesses have been calculated so that the translational and rotational bearing stiffnesses with respect to the midbearing location are the same between the distributed block stiffness and the equivalent distributed block stiffness models.

The engine block stiffness is normally not considered in crankshaft analysis unless a coupled engine block and crankshaft model is used as in the present work. An oil film hydrodynamic pressure always exists between the main journal and the engine block. This pressure extends only to a small journal arc for a heavily loaded bearing (see Figure 4). Integration of the hydrodynamic pressure results in the reaction force R which is applied on point C of the journal. Point C is crankangle dependent. If the oil film hydrodynamics are neglected, the crankshaft journal will touch the bulkhead around point C. The engine block stiffness, as seen by the crankshaft, is the local circumferential stiffness of the engine block at point C. At each time step during the dynamic simulation, the bearing reactions R depend on the local engine block stiffness which depends on the location of point C. For this reason, an iterative process is needed to calculate the bearing reactions R and their points of application C, simultaneously. In this work, a non-linear solver is used which iterates between assumed local engine block stiffnesses for each bearing and the resulting bearing reactions R until it finds points C with reasonable accuracy. For computational efficiency, the reaction R from the previous time step can also be used to estimate the local bulkhead stiffness needed at the current time step.

In summary, the vertical and horizontal engine block stiffnesses are distributed along the bearing length and can be different for each main bearing. The circumferential variation of both the vertical and horizontal stiffnesses is also considered for each bearing. These features constitute a unique engine block stiffness representation, which fully accounts for the anisotropy of the engine block flexibility as seen by a rotating crankshaft. The coupling

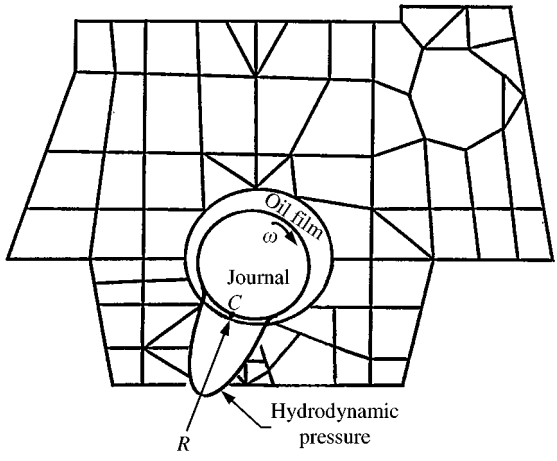

Figure 4. Representation of the actual engine block stiffness.

stiffness between the vertical and horizontal planes of the same bearing has been neglected. The coupling stiffness among different bearings has also been neglected.

5. CRANKSHAFT—ENGINE BLOCK MODEL

In order to find the dynamic response of the crankshaft–engine block system, the rotating crankshaft must be combined with the non-rotating (fixed) engine block. A common coordinate system must be used for the combined model. The crankshaft dynamic analysis described in this report assumes that the crankshaft mass and stiffness matrices are time invariant. For this reason, the analysis is performed with respect to a right-handed rotating coordinate system (x, y, z) which is attached to the crankshaft. The x coordinate points always to crankpin $\#1$ (see Figure 5) and the z coordinate is along the crankshaft axis towards the flywheel end.

The engine block stiffness is given with respect to a right-handed, non-rotating coordinate system (X, Y, Z). The X coordinate is positive upwards and the Z coordinate is along the crankshaft axis towards the flywheel end. At a crank angle θ, the coordinate transformation of Figure 5 holds between the rotating and non-rotating coordinate systems. If k_X and k_Y represent the vertical and horizontal engine block stiffnesses, respectively, in the fixed coordinate system, the engine block stiffness in the rotating coordinate system is

$$[K^b] = [T]^{\mathrm{T}} \begin{bmatrix} k_X & 0 \\ 0 & k_Y \end{bmatrix} [T] = \begin{bmatrix} k_x & k_{xy} \\ k_{yx} & k_Y \end{bmatrix}, \tag{23}$$

where

$$[T] = \begin{bmatrix} \cos\theta & -\sin\theta \\ \sin\theta & \cos\theta \end{bmatrix} \tag{24}$$

and

$$k_x = k_X \cos^2\theta + k_Y \sin^2\theta, \qquad k_y = k_X \sin^2\theta + k_Y \cos^2\theta, \tag{25a, b}$$

$$k_{xy} = k_{yx} = -k_X \cos\theta \sin\theta + k_Y \cos\theta \sin\theta. \tag{25c}$$

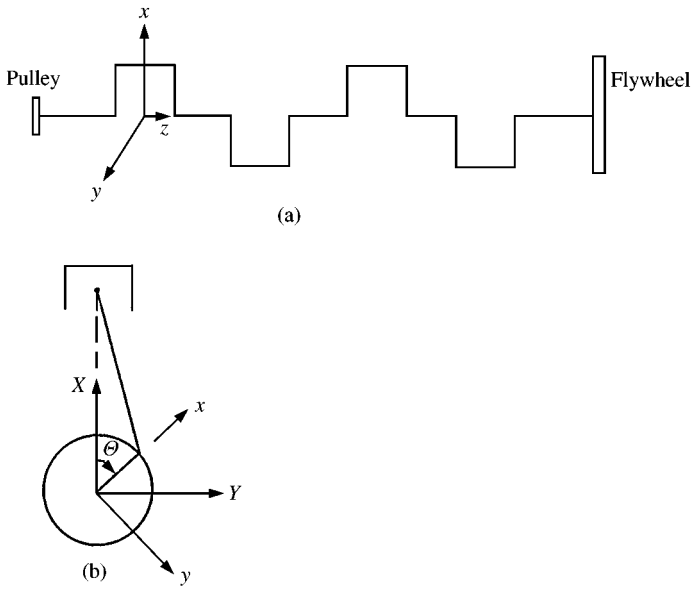

Figure 5. Definition of the rotating (x–y–z) and fixed (X–Y–Z) coordinate systems. (a) Sideview of crank, (b) front view of piston–crank mechanism. The transformation is

$$\begin{bmatrix} X \\ Y \end{bmatrix} = \begin{bmatrix} \cos\Theta & -\sin\Theta \\ \sin\Theta & \cos\Theta \end{bmatrix} \begin{bmatrix} x \\ y \end{bmatrix}$$

The matrix $[K^b]$ is added to the reduced stiffness matrix of the crankshaft to get the combined stiffness matrix for the crankshaft–engine block model. The combined stiffness matrix is crankangle dependent. If the engine block stiffness in the vertical and horizontal directions are the same ($k_X = k_Y$), $[K^b]$ is crankangle independent in the rotating coordinate system. In this case, the dynamic matrices of the reduced crankshaft–engine block model are formulated and decomposed once. This not only simplifies the analysis but also results in additional computational savings.

5.1. STRUCTURAL DAMPING

In the reduced crankshaft–engine block model of equation (14), $[\bar{C}]$ is the structural damping matrix. A particularly convenient form of $[\bar{C}]$ is the Rayleigh damping matrix

$$[\bar{C}] = \alpha[\bar{M}] + \beta[\bar{K}], \tag{26}$$

where α and β are two constants to be determined from two specified damping ratios which correspond to two unequal natural frequencies of the system. If has been shown [29] that if the system eigenvectors are $[C]$-orthogonal, the following equation holds:

$$\alpha + \beta\omega_i^2 = 2\zeta_i\omega_i, \tag{27}$$

where ω_i is the ith natural frequency of the system and ζ_i is the damping ratio for the ith mode. Given the natural frequencies and damping ratios of two different modes, the coefficients α and β can be determined by solving equation (27). Subsequently, equation (27)

can be used to calculate ζ_i at any frequency ω_i. The Rayleigh damping is a computationally convenient way to approximate the actual structural damping.

5.2. CRANKSHAFT LOADING

The crankshaft is mainly loaded by the engine operating load which comes from the cylinder combustion. This load is transmitted through the piston and connecting rod to the crankpin. The piston and the connection rod are treated as rigid bodies and their inertia loads are calculated and combined with the combustion load. The combined load is applied on the crankpin in the rotating coordinate system. The belt loads are also applied on the crankshaft. Since the analysis is performed in the rotating coordinate system, the crankshaft inertia load due to centrifugal forces is also applied on the crankshaft. For a particular finite element model of the crankshaft, this inertia load is equal to $mr\omega^2$, where m is the mass of the solid element, r is the distance of its center of gravity from the crankshaft rotating axis and ω is the crankshaft rotational velocity. The coriolis forces are neglected.

5.3. CRANKSHAFT "BENT" AND ENGINE BLOCK MISBORING

Crankshaft "bent" and engine block misboring (see Figure 6) represent manufacturing imperfections. The forging, heat treating and machining operations necessary to produce a crankshaft sometimes produce a slightly bent crankshaft. Since this effect is expected, the crankshaft is subsequently straightened so that it conforms to certain finished tolerances. However, it is very difficult to straighten the crankshaft perfectly.

Similarly, the main bearings in the block structure may lie on different centerlines due to slight misboring. It has been found [30] that significant bearing loads were induced when bearings 1 and 4 of a six-throw engine were 0·02 mm below the common centerline. The effect of both crankshaft "bent" and engine block misboring are included in the formulation of the combined crankshaft–engine block model which is presented next.

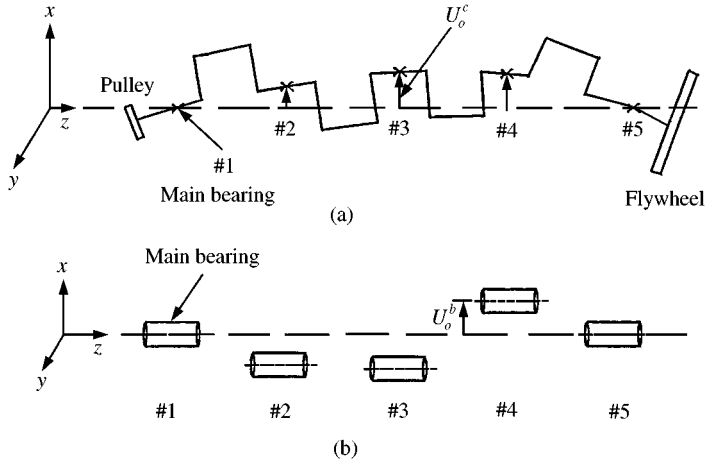

Figure 6. (a) Schematic of crankshaft "bent", (b) schematic of engine block misboring.

5.4. FORMULATION OF THE CRANKSHAFT–ENGINE BLOCK MODEL

The reduced crankshaft model is described in the rotating coordinate system by

$$[M^c]\{\ddot{u}^c\} + [C^c]\{\dot{u}^c\} + [K^c]\{u^c\} = \{F^c\}, \tag{28}$$

where

$$\{u^c\} = \{u_i^c \,|\, U_r^c\}^{\mathrm{T}}, \tag{28a}$$

where $\{u_i^c\}$ is the generalized displacement vector after second level of substructuring, $\{U_r^c\}$ the crankshaft retained (subscript r) displacement vector, and $\{F^c\}$ the vector of applied forces on the crankshaft.

The superscript c denotes the crankshaft in the above quantities. The engine block model is described in the rotating coordinate system by

$$[C^b]\{U_r^b\} + [K^b]\{U_r^b\} = \{F^b\}, \tag{29}$$

where $\{U_r^b\}$ is the block retained (subscript r) displacement vector, and $\{F^b\}$ the vector of applied forces on the block.

Superscript b denotes the block in the above quantities.

The mass inertia effect is neglected for the block model. The block stiffness matrix $[K^b]$ is given in the rotating coordinate system by equation (23). The block damping matrix $[C^b]$ is similarly defined. Inclusion of the block damping is necessary because it dampens any crankshaft free-body motion.

Let

$$\{U_T^c\} = \{U_o^c\} + \{U_r^c\}, \qquad \{U_T^b\} = \{U_o^b\} + \{U_r^b\}, \tag{30a, b}$$

where U_T^c, U_T^b are the total (subscript T) displacements of the crankshaft and block, respectively, relative to a straight reference line at the mains (see Figures 6(a) and 6(b), including elastic deformation. U_o^c, U_o^b are the crankshaft "bent" and engine block misboring, respectively. They are known deviations or offsets (subscript o) from the same reference line. U_r^c, U_r^b are the crankshaft and the block retained displacement vectors, respectively. They represent the elastic deformation of the crankshaft and block from their undeformed position.

All the above vectors include the crankshaft and block displacements at the left end, middle position and right end of each main bearing. The reference line needed to define the vectors is arbitrarily taken as a straight line passing through the middles of the first (fan end) and the last (flywheel) bearings. The offsets of the first and last bearings are arbitrarily set to zero. The "runout" of the other bearings, or the amount they deviate from that straight line in the rotating crankshaft coordinate system are then entered as offsets. The engine block misboring is specified in a similar way but in a fixed coordinate system.

Based on the partitioning of equation (22a), equation (28) can be written as

$$\begin{bmatrix} M_{ii}^c & M_{ir}^c \\ M_{ir}^{cT} & M_{rr}^c \end{bmatrix} \begin{bmatrix} \ddot{u}_i^c \\ \ddot{U}_r^c \end{bmatrix} + \begin{bmatrix} C_{ii}^c & C_{ir}^c \\ C_{ir}^{cT} & C_{rr}^c \end{bmatrix} \begin{bmatrix} \dot{u}_i^c \\ \dot{U}_r^c \end{bmatrix} + \begin{bmatrix} K_{ii}^c & K_{ir}^c \\ K_{ir}^{cT} & K_{rr}^c \end{bmatrix} \begin{bmatrix} u_i^c \\ U_r^c \end{bmatrix} = \begin{bmatrix} F_i^c \\ F_r^c \end{bmatrix}. \tag{31}$$

The bearing eccentricity is defined as the difference of the total displacements of the crankshaft and block at the bearing locations,

$$\{\varepsilon\} = \{U_T^c\} - \{U_T^b\}, \tag{32}$$

or due to equation (30),

$$\{U_r^b\} = \{U_o^c\} - \{U_o^b\} + \{U_r^c\} - \{\varepsilon\}. \tag{33}$$

Also due to the action and reaction principle,

$$\{F_r^c\} = -\{F^b\}. \tag{34}$$

Combining equations (29), (33) and (34) yields

$$\{F_r^c\} = [C^b](\{\dot{\varepsilon}\} + \{\dot{U}_o^b\} - \{\overset{0}{\dot{U}}_o^c\}) + [K^b](\{\varepsilon\} + \{U_o^b\} - \{U_o^c\}) - [C^b]\{\dot{U}_r^c\} - [K^b]\{U_r^c\}. \tag{35}$$

Since the crankshaft "bent" $\{U_o^c\}$ is a vector of constants in the rotating coordinate system, its time derivative is always equal to zero. However, since the block misboring $\{U_o^b\}$ is given in the fixed coordinate system, it must be transformed to the rotating coordinate system using equation (24). Due to that transformation, its time derivative is not zero unless the block misboring has the same value in the vertical and horizontal directions at each bulkhead location. Substitution of equation (35) into equation (31) gives

$$\begin{bmatrix} M_{ii}^c & M_{ir}^c \\ M_{ir}^{cT} & M_{rr}^c \end{bmatrix} \begin{bmatrix} \ddot{u}_i^c \\ \ddot{U}_r^c \end{bmatrix} + \begin{bmatrix} C_{ii}^c & C_{ir}^c & \\ C_{ir}^{cT} & C_{rr}^c + & C^b \end{bmatrix} \begin{bmatrix} \dot{u}_i^c \\ \dot{U}_r^c \end{bmatrix} + \begin{bmatrix} K_{ii}^c & K_{ir}^c & \\ K_{ir}^{cT} & K_{rr}^c + & K^b \end{bmatrix} \begin{bmatrix} u_i^c \\ U_r^c \end{bmatrix} = \begin{bmatrix} F_i^c \\ F^* \end{bmatrix}, \tag{36a}$$

where

$$\{F^*\} = [C^b](\{\dot{\varepsilon}\} + \{\dot{U}_o^b\}) + [K^b](\{\varepsilon\} + \{U_o^b\} - \{U_o^c\}). \tag{36b}$$

If the bearing hydrodynamics are neglected $\{\varepsilon\} = 0$. However, even in this case, the crankshaft "bent" and block misboring produce equivalent forces according to equation (36b)), which are applied on the crankshaft. All the quantities in equation (36) must be expressed in the rotating coordinate system.

Equation (36) are integrated in time (or crankangle) to find the response of the reduced system. Before this is done, a torsional boundary condition is applied at the flywheel end of the crankshaft to eliminate the rotational free-body motion. The Newmark method [31] is used for the time integration. At each time step, equation (33) is used to calculate the block deflection $\{U_r^b\}$ and equation (29) is subsequently used to calculate the bearing reaction forces and moments.

Equation (36) gives the dynamic displacements of the reduced crankshaft–engine block system model. The displacements of the original crankshaft model can be obtained by two backwards transformations (one for each level of substructuring) given by equation (13). The displacements of the original model can be subsequently be processed to calculate the crankshaft operating dynamic stresses.

6. SELECTED RESULTS AND DISCUSSION

In this section, the accuracy and efficiency of the developed method is first demonstrated by comparison with MSC/NASTRAN Version 67.0. MSC/NASTRAN was used with and without dynamic reduction. When dynamic reduction was performed in MSC/NASTRAN,

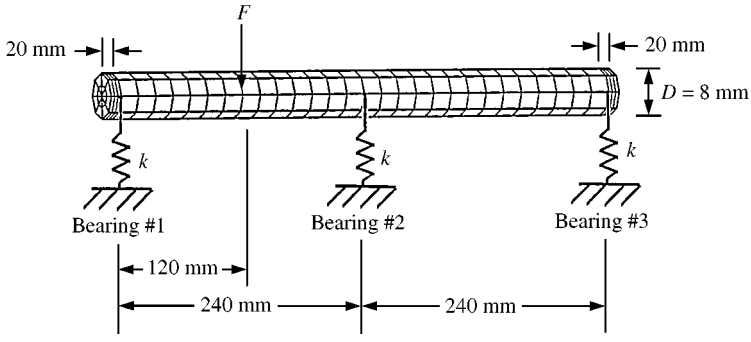

Figure 7. Schematic of the three-bearing slender cylindrical beam.

the component mode synthesis (CMS) was utilized with the transformation basis consisting of eigenvectors calculated with the Lanczos algorithm [26]. Two examples are used; a slender cylindrical beam (section 6.1) and a four-cylinder engine crankshaft (section 6.2). Both free and forced vibration results of the slender beam are presented. Free vibration analysis of the engine crankshaft further illustrates the accuracy and efficiency of the present method. All computer simulations were performed on a CRAY M98 computer. The accuracy of the present method in calculating the dynamic response of engine crankshafts is further illustrated through comparisons with experimental results from the torsional vibrations of an in-line five-cylinder engine (section 6.3) and the bending vibrations of the crankshaft–flywheel assembly of a V6 engine (section 6.4).

6.1. SLENDER CYLINDRICAL BEAM

A schematic of the cylindrical beam is shown in Figure 7. The beam is supported by three equally spaced bearings and is loaded in the middle of the first two bearings by a concentrated force. It is 480 mm long and has a diameter of 8 mm. Each bearing is represented by a concentrated stiffness $k = 40\,000$ N/mm. The beam was discretized into 4480 solid finite elements using 4777 nodes. Although this discretization is very fine for calculating the dynamic response of the beam, it was chosen in order to minimize the discretization errors in the results. Furthermore, since the number of nodes between two bearings is representative of that used in modelling an engine crankshaft bay (structure between two adjacent bearings), it is expected that the computational effort will be comparable to that of an actual engine crankshaft.

The first 15 non-zero natural frequencies of the free–free (unsupported) beam are presented in Table 1. The present analysis and the MSC/NASTRAN superelement analysis (Sol. 103) were used to calculate the natural frequencies of the beam. The "exact" natural frequencies are also presented in the table for comparison reasons. They were calculated using MSC/NASTRAN on the whole beam model (no superelements). Due to the fine discretization, the calculated natural frequencies are expected to be accurate. For this reason, they are marked "exact". Since the beam is symmetric, the natural frequencies appear in pairs. In Table 1, however, only the distinct natural frequencies are presented. Two levels of superelement analysis were used in MSC/NASTRAN, similar to the two levels of dynamic reduction used in the present method. Nine and 20 basis vectors were used. A basis vector is a Ritz vector or an eigenvector for the present analysis and MSC/NASTRAN analysis respectively. Only the accurately calculated natural frequencies

TABLE 1

Non-zero natural frequencies of the free–free cylindrical beam in Hz

		9 basis vectors		20 basis vectors	
No.	"Exact"	MSC/ NASTRAN	Present analysis	MSC/ NASTRAN	Present analysis
1	126·8	126·8	126·8	126·8	126·8
2	349·4	349·5	349·4	349·4	349·4
3	684·0	687·0	684·2	684·2	684·0
4	1128·7	1129·3	1128·8	1128·7	1128·7
5	1682·2	1727·4	1685·8	1684·2	1682·5
6	2343·2		2344·6	2343·6	2343·6
7	3035·4		3089·7	3111·0	3039·9
8	3109·9		3207·4	3127·6	3111·4
9	3980·5		3991·3	3987·2	3982·5
10	4868·9		4954·5		4870·3
11	4952·7		4963·7		4958·1
12	6024·3				6030·1
13	6070·8				6117·5
14	7192·7				7211·5
15	8455·4				8497·7

are presented in Table 1. If the error in calculating a particular natural frequency exceeded 3 percent, the corresponding entry in Table 1 was left blank. As shown in Table 1, the present analysis calculated accurately a larger number of natural frequencies both with nine and 20 basis vectors. Furthermore, the present analysis with nine basis vectors calculated 11 natural frequencies accurately versus nine of MSC/NASTRAN with 20 basis vectors. This is the first indication that superior accuracy can be achieved with the present analysis even with a much smaller number of basis vectors. This translates to reduced computational effort as compared to an equivalent MSC/NASTRAN superelement analysis.

Figure 8 presents a CPU time comparison between the present analysis and MSC/NASTRAN for the free–free beam. Four separate cases are considered; an MSC/NASTRAN Solution 103 analysis of the whole model without superelements (NASTRAN; Whole Model), an MSC/NASTRAN Solution 103 superelement analysis (NASTRAN; Superelements), a present analysis using Ritz vectors (PRESENT; Ritz vectors) and a present analysis using eigenvectors (PRESENT; Eigenvectors). In the first case, a modal reduction of the whole beam was performed, while in the second case a two-level superelement reduction was performed. In the last case, instead of using the Ritz transformation in the present analysis, the conventional modal transformation was used similar to MSC/NASTRAN superelement analysis. This will allow a more fair comparison of the Ritz vector approach with the conventional eigenvector approach through the same analysis procedure. Again nine and 20 basis vectors were used. As shown in Figure 8, the MSC/NASTRAN superelement analysis is always the most expensive while the present analysis with the Ritz vectors is always the least expensive. The MSC/NASTRAN superelement analysis is almost twice as expensive as the present Ritz analysis. The MSC/NASTRAN modal analysis of the whole model is 51 and 32 per cent more expensive than the present Ritz analysis for nine and 20 basis vectors respectively. The present eigenvector analysis is 25 and 12 per cent more expensive than the present Ritz analysis for nine and 20 basis vectors respectively. The present Ritz analysis with 20 basis vectors is

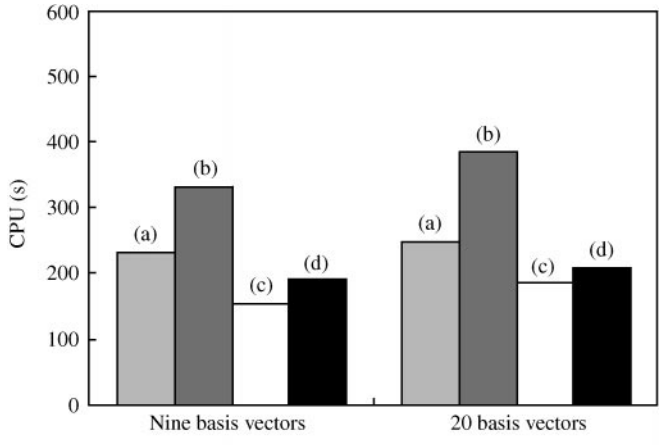

Figure 8. Comparison of CPU time in calculating the natural frequencies of the free–free cylindrical beam. (a) NASTRAN, whole model; (b) NASTRAN, superelements; (c) PRESENT, Ritz vectors; (d) PRESENT, eigenvectors.

TABLE 2

Non-zero natural frequencies of the supported cylindrical beam in Hz

		9 basis vectors		20 basis vectors	
No.	"Exact"	MSC/ NASTRAN	Present analysis	MSC/ NASTRAN	Present analysis
1	261·9	261·9	261·9	261·9	261·9
2	406·4	406·4	406·4	406·4	406·4
3	1037·1	1037·6	1037·4	1037·1	1037·1
4	1289·8	1292·3	1290·1	1289·9	1289·8
5	2295·8		2298·5	2296·2	2295·9
6	2605·3		2609·5	2608·0	2605·5
7	3035·3		3090·1	3049·1	3039·9
8	3980·3			3988·1	3982·3
9	4241·1			4254·2	4243·4
10	4868·9				4870·3
11	5649·8			5693·0	5677·7
12	5705·1				5735·0
13	6070·8				6117·3
14	6558·0				6576·8
15	8512·3				8541·2
16	8865·2				8897·4

almost as expensive as the present eigenvector analysis with nine basis vectors. In summary, based on Table 1 and Figure 8, the present Ritz analysis is the most accurate and least expensive method for the free beam example.

The superior accuracy of the present Ritz analysis is further demonstrated in Table 2 and Figures 10 and 11 for the supported slender cylindrical beam. Table 2 presents the first 16 non-zero natural frequencies. The arrangement of results is similar to that of Table 1. Again the present Ritz analysis is more accurate than MSC/NASTRAN superelement analysis in the sense that it calculates accurately a larger number of natural frequencies. The CPU time comparison is exactly the same with the free–free beam and therefore not presented here.

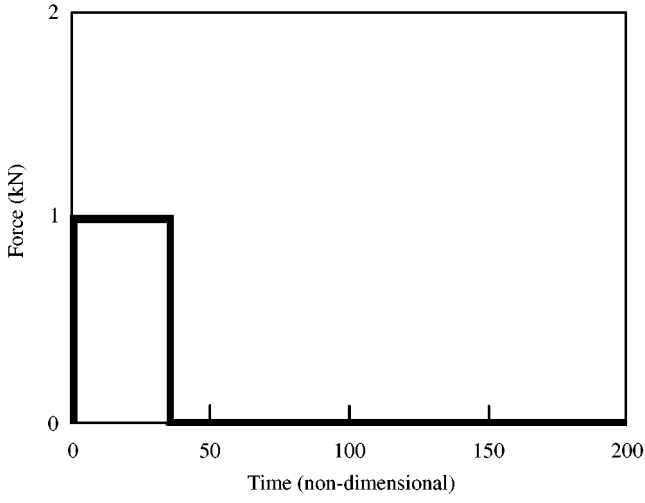

Figure 9. Vertical loading of the cylindrical beam.

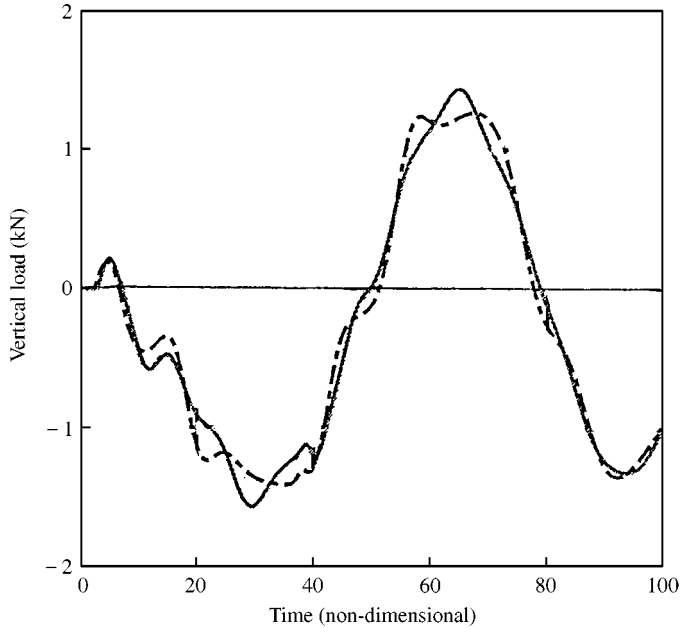

Figure 10. Reaction of bearing #2 of the cylindrical beam calculated by the present method: ——, 20 Ritz vectors; …, nine Ritz vectors; - - - - -, five Ritz vectors.

Figures 10 and 11 illustrate the accuracy of the present analysis for a forced vibration case of the supported cylindrical beam. The beam is loaded in the middle of the first bay by a vertical force F (see Figure 7). A step force F of 1 kN magnitude and duration of 35 non-dimensional time units, as shown in Figure 9, is used. Figure 10 shows the bearing #2 reaction force as calculated by the present method with five, nine and 20 Ritz vectors. Although not shown in the figure, the bearing reaction is almost exact throughout the non-dimensional time range, when 20 Ritz vectors are used. It is also exact with only nine Ritz

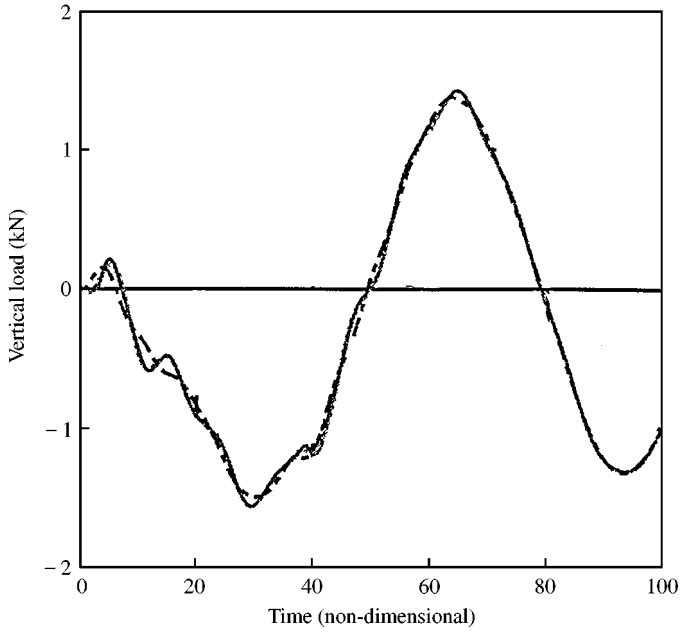

Figure 11. Reaction of bearing #2 of the cylindrical beam calculated by MSC/NASTRAN superelement analysis: ——, "exact", ·····, 15 eigenvectors; ----- nine eigenvectors.

vectors. However, five Ritz vectors are not enough to give the same good accuracy. In Figure 11, the bearing #2 reaction force has been calculated using MSC/NASTRAN superelement analysis with nine and 15 eigenvectors. Although 15 eigenvectors give almost exact results, nine eigenvectors do not provide the same accuracy. Recall that the nine Ritz vectors gave exact results (Figure 10). Therefore, if the same number of Ritz vectors is used instead of eigenvectors, superior accuracy is achieved.

6.2. ENGINE CRANKSHAFT

A free vibration analysis was also performed on a four-cylinder engine crankshaft in order to demonstrate the superiority of the Ritz vector approach in dynamic analysis of actual engine crankshafts. The finite-element mesh is shown in Figure 12. The pulley and the flywheel are also included in the model. The mesh consists of 4498 solid elements and 6504 grids with a total of 19 512 d.o.f.s.

Table 3 presents the first 17 non-zero natural frequencies of the crankshaft as calculated by the present analysis and MSC/NASTRAN superelement analysis with four and seven basis vectors. The "exact" natural frequencies are also presented for comparison. The table is arranged in the same way with Tables 1 and 2. It is shown that the present analysis calculates accurately a larger number of natural frequencies than MSC/NASTRAN does both with four and seven basis vectors. Furthermore, the present analysis with four basis vectors calculates accurately more natural frequencies than MSC/NASTRAN does with seven basis vectors.

A CPU time comparison between the present analysis and MSC/NASTRAN superelement analysis for an in-line, four-cylinder engine crankshaft is shown in Figure 13. Three different cases are presented; the present analysis with Ritz vectors and eigenvectors

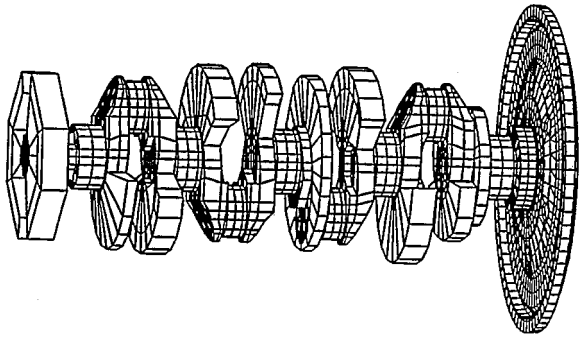

Figure 12. Finite-element mesh for a four-cylinder engine crankshaft.

TABLE 3

Non-zero natural frequencies of the free–free engine crankshaft in Hz

		4 basis vectors		7 basis vectors	
No.	"Exact"	MSC/ NASTRAN	Present analysis	MSC/ NASTRAN	Present analysis
1	163·8	163·9	163·7	163·9	163·9
2	176·1	176·1	176·1	176·1	176·1
3	236·1	236·6	237·0	236·6	236·5
4	282·1	283·2	283·2	283·1	283·1
5	386·1	388·0	387·3	388·0	387·9
6	396·7	397·8	396·0	396·9	396·9
7	397·6	404·1	401·1	404·1	404·1
8	421·3		425·3	425·9	425·0
9	502·1		502·7	509·7	503·4
10	619·9		593·5		625·2
11	668·6		665·9		673·7
12	793·2		785·3		802·4
13	896·1				873·2
14	1067·6				1081·1
15	1070·3				1086·3
16	1073·4				1100·5
17	1097·3				

and an MSC/NASTRAN two-level superelement analysis. In all three cases, four, seven and 25 basis vectors are used. The present analysis with Ritz vectors requires the least CPU time while the MSC/NASTRAN analysis requires the most. This is in accordance with the CPU time comparisons for the cylindrical beam (see Figure 8). MSC/NASTRAN needs 76, 69 and 24 per cent more CPU time than the present Ritz analysis for four, seven and 25 basis vectors respectively. Although the CPU time for the present eigenvector analysis is less than that of MSC/NASTRAN, it is however, higher than the CPU time for the present Ritz analysis by 46, 43 and 10 percent for four, seven and 25 basis vectors respectively. MSC/NASTRAN is more expensive than the present eigenvector analysis due to certain overhead it has as a general purpose program. However, as observed from numerical experimentations not presented in this work, the results of the present eigenvector analysis

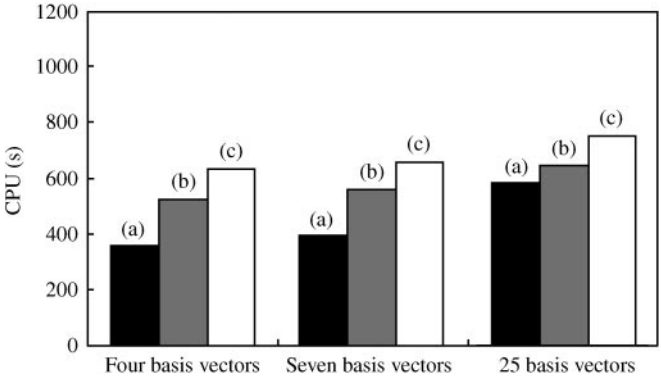

Figure 13. Comparison of CPU time in calculating the natural frequencies of the free–free engine crankshaft. (a) PRESENT, Ritz vectors; (b) PRESENT, eigenvectors; (c) NASTRAN, superelements.

are identical with MSC/NASTRAN when the number of reduction levels and the number of eigenvectors used for each reduction are the same for the two analyses. It should be pointed out (see Figure 13) that the present Ritz analysis with 25 basis vectors requires less CPU time than MSC/NASTRAN does with four basis vectors. This is one more indication of the superior efficiency of the present Ritz analysis.

6.3. DYNAMIC ANALYSIS OF AN IN-LINE FIVE-CYLINDER ENGINE

In order to experimentally validate the accuracy of the proposed methodology, the dynamic analysis of a five-cylinder in-line (L5) engine crankshaft was performed using the finite-element based analytical tool CRANKSYM which implements the methodology presented in this paper. The response of the L5 crankshaft under wide-open-throttle (WOT) operating conditions was simulated and correlated with measurements.

Figures 14 and 15 show the measured and computed angular vibrations of the L5 crankshaft, respectively, in "waterfall" format. The torsional vibration amplitude in degrees is plotted for different engine orders and engine speeds. Note that the measured and simulated vibration amplitudes are peak to peak and single amplitude (half to peak to peak) respectively. There is a very good correlation between the simulated vibrations with CRANKSYM and the measured vibrations at all engine speeds except around 6200 r.p.m. at 2·5 engine order where CRANKSYM's prediction is about 20% higher than the measurement. The difference is mainly due to two reasons. First, the inherent non-linearity of the tuned torsional vibration absorber's elastomer and second the coupling between the absorber's inertia ring and the accessory drive components.

The behavior of the non-linear tuned absorber is such that higher vibration amplitudes would decrease the stiffness and increase the damping of the elastomer. This change in the elastomer material properties with deformation results in a decrease of the crankshaft resonance frequency and an increase of the crankshaft damping. The conducted simulations did not consider the non-linear effects of the tuned absorber elastomer and therefore, such small differences between simulated and measured vibrations were expected.

The accessory drive components were found to interact with the tuned absorber's inertia ring since the latter is used as a pulley. This interaction seems to manifest itself as a decrease in the inertia of the ring, which effectively increases the tuning frequency of the absorber. This inertia reduction effect was calculated and included in the simulations by decreasing

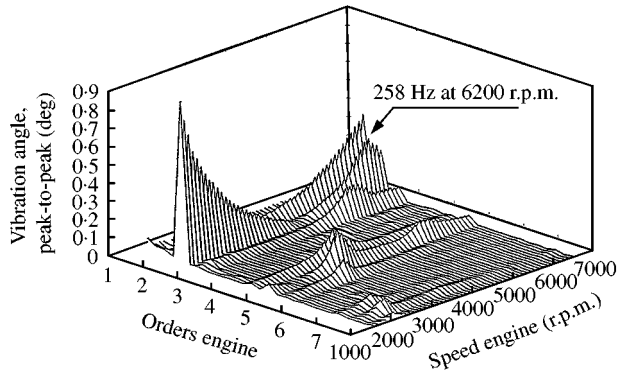

Figure 14. Measured engine crankshaft torsional vibration for an in-line, five-cylinder engine.

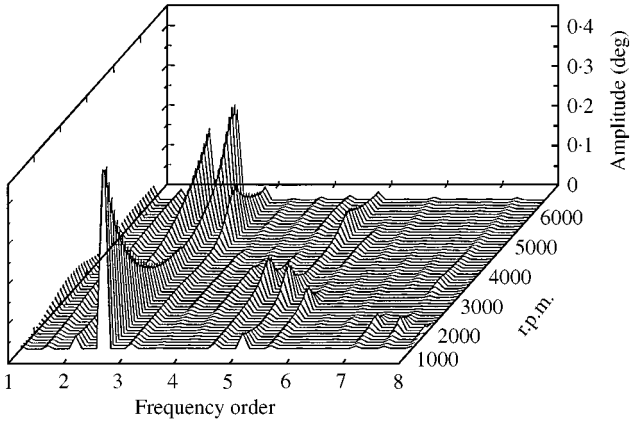

Figure 15. Simulated engine crankshaft torsional vibration for an in-line, five-cylinder engine.

the ring's inertia and increasing the tuning frequency of the absorber appropriately. The effect of the accessory drive components on the effective inertia of the absorber's ring can be significant and depends on which accessory components are present and whether A/C is engaged.

In order to eliminate the inherent non-linearity of the tuned torsional vibration absorber's elastomer, the absorber's ring was pinned to the hub (locked ring), deactivating, therefore, the effect of the elastomer's damping. Furthermore, the coupling between the absorber's inertia ring with the accessory drive components, was eliminated by disconnecting the accessory drives from the crank pulley in a control dynamometer test. Figures 16 and 17 show the measured and computed angular vibrations of the L5 crankshaft respectively in this case. The agreement now is excellent. Note also that the peaks of the resonances are more pronounced since the absorber's damping is eliminated.

6.4. CRANKSHAFT–FLYWHEEL BENDING VIBRATIONS OF A V6 ENGINE

High vibration levels at the rear bearing cap and oil pump were observed in dynamometer tests for a particular design of a V6 engine at a rated speed of 4800 r.p.m. The

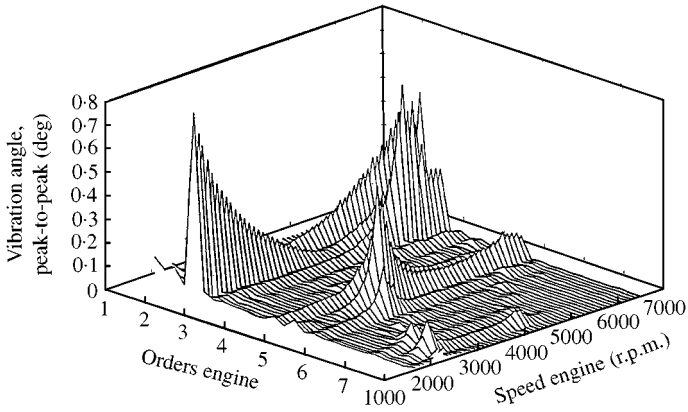

Figure 16. Measured engine crankshaft torsional vibration for an in-line, five-cylinder engine with locked absorber's ring.

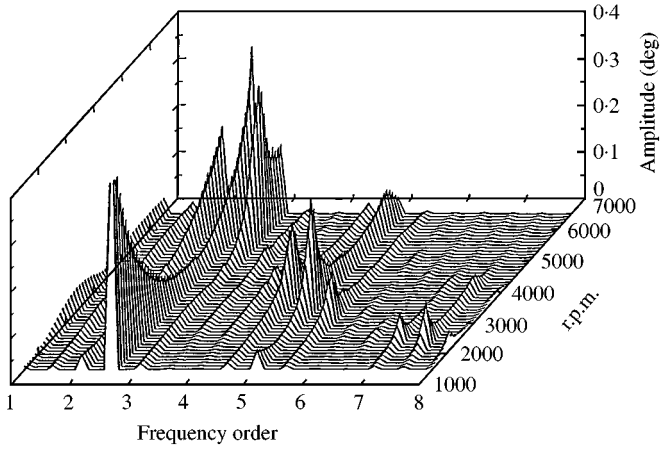

Figure 17. Simulated engine crankshaft torsional vibration for an in-line, five-cylinder engine with locked absorber's ring.

axial (along the crankshaft axis) vibratory displacement of a point on the flywheel rim was measured relative to crankshaft fixed coordinates. The measured vibratory results are presented in "waterfall" format (Figure 18). It was evident from the experimental results that the crankshaft–flywheel assembly had a bending resonance at 240 Hz which was excited at around 4800 r.p.m. by third order forces on the crankshaft. CRANKSYM was used to analytically verify the above finding and propose possible solutions. The finite-element mesh of the crankshaft–flywheel assembly consisted of approximately 3650 grids and 2330 solid elements. The structure was supported by linear springs and dampers at the main bearing locations representing the engine block stiffness and damping. Due to lack of actual data, a 300 300 N/mm block stiffness was assumed for each bulkhead both in the vertical and lateral directions. A crankshaft structural damping of less than 1 per cent of critical was used. The block structural damping was taken equal to 3 per cent of critical throughout the whole frequency range. Lubrication analysis of the main bearings was not included.

The following three designs were examined with CRANKSYM. First, the baseline design which was an externally balanced crankshaft with a balancing weight on the flywheel (denoted BASELINE). Second, an internally balanced crankshaft with the relatively heavy

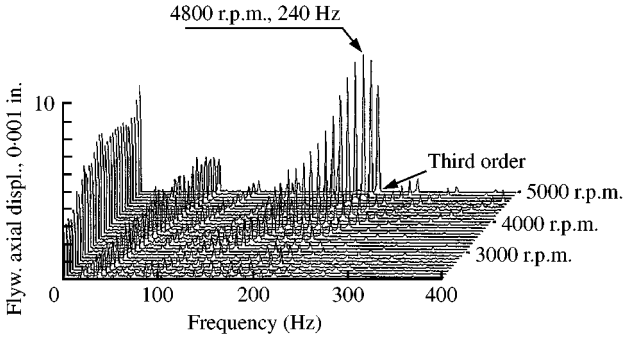

Figure 18. Flywheel axial vibratory displacement relative to crankshaft-fixed coordinates.

TABLE 4

Calculated natural frequencies for the crankshaft–flywheel assembly

	f_1 (Hz)	f_2 (Hz)	f_3 (Hz)	f_4 (Hz)
BASELINE	219	252	339	414
HEAVYPIS	211	247	338	413
LIGHTMAS	287	322	372	427

baseline pistons (denoted HEAVYPIS) and third, an internally balanced crankshaft with the "heavy" baseline pistons but with 50 per cent flywheel mass and therefore, 50 per cent inertia (denoted LIGHTMAS). The dynamic response of the three designs was calculated for the range of 4000–5000 r.p.m. with a 200 r.p.m. increment. At each r.p.m. a separate program was used to calculate the crank pin load for all cylinders at each crankangle. This load included both the gas pressure load and the inertia load for each cylinder, with the appropriate phasing. The axial displacement of the flywheel was calculated in a rotating with the crankshaft coordinate system, since in this case the flywheel axial motion reveals the actual frequency content of the crankshaft–flywheel vibration. The flywheel vibration is shifted by one order if the flywheel displacement is calculated in a fixed coordinate system. The axial flywheel motion was also measured in a rotating coordinate system.

Table 4 presents the first four natural frequencies of the crankshaft–flywheel assembly for the three designs as calculated by CRANKSYM. The lowest natural frequency of the baseline design was found to be 219 Hz which is lower than the experimentally found frequency of 240 Hz (see Figure 18). The discrepancy is most likely due to the fact that the assumed block stiffness of 300 000 N/mm may not be accurate enough. From results not presented in this paper, it was found that the lowest natural frequency can be increased by 15 Hz if the rear bulkhead stiffness is increased by an order of three.

Figure 19 compares the flywheel axial displacement throughout the engine cycle at 4800 r.p.m. for the BASELINE and HEAVYPIS designs. Both curves are similar in shape. However, the mean axial displacement of HEAVYPIS is much closer to the equilibrium value of zero. This indicates that the flywheel bending displacement is greatly reduced if the crankshaft is internally balanced. Note that small flywheel bending displacement yields small axial displacement. From the design standpoint, small mean flywheel axial displacement is desirable since it will reduce the dynamic load on the rear main bearing.

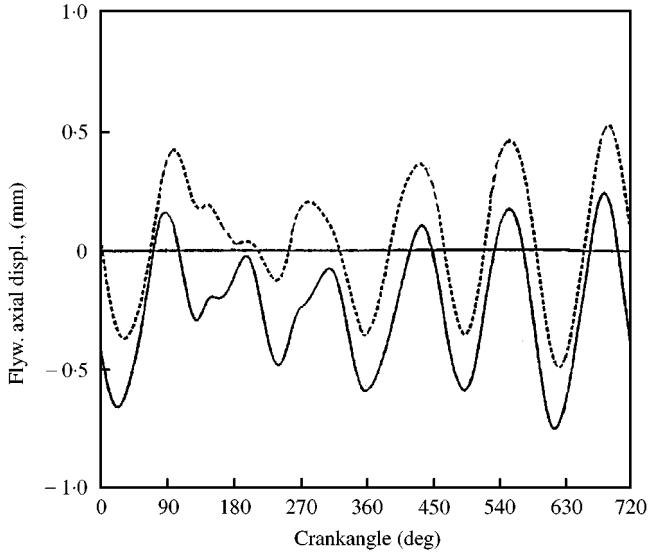

Figure 19. Comparison of flywheel axial displacement at 4800 r.p.m.: ——, baseline, extenal balancing (avrg value = − 0·2411); - - - - -, heavypis; internal balancing (avrg value = 0·0415).

TABLE 5

Fourier analysis of flywheel axial displacement (*in millimeters*) *for the BASELINE case; external balance*

	Order number k					
r.p.m	0	2	2·5	3	3·5	4
4000	0·170	0·035	0·074	0·199	0·106	0·049
4200	0·186	0·039	0·087	0·411	0·069	0·035
4400	0·204	0·043	0·104	0·607	0·065	0·027
4600	0·222	0·049	0·131	0·418	0·046	0·021
4800	0·240	0·055	0·177	0·292	0·032	0·018
5000	0·259	0·063	0·266	0·232	0·023	0·015

The baseline axial displacement of Figure 19 has six peaks and six valleys through the engine cycle. This is indicative of a strong sixth-harmonic component or equivalently, a strong third order component. The Fourier analysis results of the BASELINE flywheel axial displacement are shown in Table 5. The magnitude of the displacement at each order and r.p.m. is given in millimeters. At each r.p.m., there is a large mean component (zeroth order) and a large third order component. Both findings are consistent with the experimental results of Figure 18. The third order resonance occurs at 4400 r.p.m. and has a maximum axial displacement of 0·607 mm. Since the excitation frequency in Hz is $f = \text{r.p.m.} * \text{engine}/60$, f equals to 220 Hz at 4400 r.p.m. This is a resonance condition with the first natural frequency of 219 Hz (see Table 4) of the BASELINE design. It is also shown in Table 5 that the 2·5 order component of the axial displacement has a sizable magnitude of 0·266 mm at 5000 r.p.m. Since the corresponding excitation frequency $f = 5000 * 2{\cdot}5/60 =$ 208·5 Hz is close to the 219 Hz natural frequency, a 2·5 order resonance at a little higher

than 5000 r.p.m. will also occur. However, the magnitude of that resonance will be much lower than the third order magnitude of 0·607 mm.

The Fourier analysis of the HEAVYPIS flywheel axial displacement is shown in Table 6. Unlike the previous case, the zero order component is small. A third order resonance appears now at 4200 r.p.m. since the first natural frequency has dropped to 211 Hz and the excitation frequency is $f = 4200 * 3/60 = 210$ Hz. The magnitude of this resonance is 0·592 mm which is close to the magnitude of the third order BASELINE resonance. Again, a sizable 2·5 order resonance appears at a little higher than 5000 r.p.m.

Figure 20 compares the vertical load for main bearing #4 (rear main) at 4800 r.p.m. for the BASELINE and HEAVYPIS designs. The maximum load reduces from 31·6 (BASELINE) to 21·7 kN (HEAVYPIS); a 31·3 per cent reduction. The comparison between BASELINE and HEAVYPIS indicates that balancing the crankshaft internally, greatly reduces the mean bending vibration amplitude (zeroth order) of the flywheel (see Figure 19),

TABLE 6

Fourier analysis of flywheel axial displacement (*in millimeters*) *for the HEAVYPIS case; internal balance*

	Order number k					
r.p.m.	0	2	2·5	3	3·5	4
4000	0·025	0·037	0·085	0·312	0·073	0·041
4200	0·029	0·042	0·103	0·592	0·063	0·031
4400	0·032	0·047	0·131	0·417	0·053	0·024
4600	0·036	0·054	0·179	0·275	0·038	0·020
4800	0·041	0·062	0·279	0·217	0·028	0·017
5000	0·046	0·073	0·464	0·182	0·021	0·015

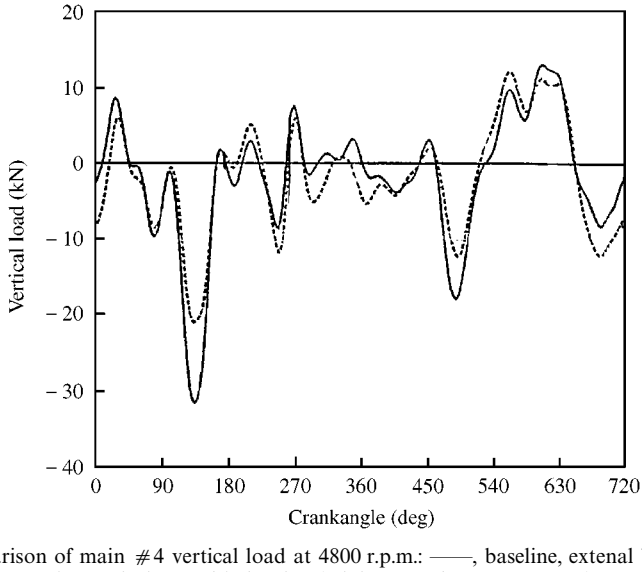

Figure 20. Comparison of main #4 vertical load at 4800 r.p.m.: ——, baseline, extenal balancing (minimum value = – 31·6519); - - - - -, heavypis, internal balancing (minimum value = – 21·1721).

TABLE 7

Fourier analysis of flywheel axial displacement (in millimeters) for the LIGHTMAS case; internal balance, 50 per cent fly wheel inertia

	Order number k					
r.pm.	0	2·5	3	3·5	4	4·5
4000	0·017	0·047	0·068	0·056	0·133	0·024
4200	0·019	0·050	0·085	0·067	0·234	0·023
4400	0·020	0·054	0·107	0·086	0·245	0·034
4600	0·021	0·058	0·140	0·121	0·151	0·029
4800	0·021	0·062	0·188	0·192	0·130	0·029
5000	0·022	0·067	0·263	0·201	0·093	0·029

resulting in a large reduction of the rear main load (see Figure 20). However, internal balancing does not eliminate, or even reduce, the third order resonance (see Tables 5 and 6).

In order to push the resonance to a higher order and therefore, reduce the amplitude of vibration, a reduced flywheel mass design (LIGHTMAS) was studied. The flywheel mass was artificially reduced to 50 per cent of the original mass, thus reducing the flywheel inertia by the same amount. The crankshaft was internally balanced with the baseline "heavy" pistons. The LIGHTMAS and HEAVYPIS cases were compared in order to demonstrate potential improvements to the flywheel dynamics due to reduced flywheel inertia. Table 4 indicates a considerable increase in the first natural frequency from 211 to 287 Hz. Table 7 gives the Fourier analysis of the flywheel axial displacement. Again, the zero order displacement is small since the crankshaft is internally balanced. There is a fourth order resonance at 4400 r.p.m. with a 0·245 mm magnitude. This magnitude is less than half the third order resonant magnitude of 0·592 mm for the HEAVYPIS case. Therefore, moving the resonant order higher reduces the magnitude of vibration, as expected. As shown in Table 7, there is also a 3·5 order resonance around 5000 r.p.m. ($f = 5000 * 3{\cdot}5/60 = 291{\cdot}7$ Hz). Also, the third order magnitude increases with increasing r.p.m., indicating that a third order resonance will appear at a little higher than 5000 r.p.m. For both those resonances, the vibration magnitude is less than half the third order resonant magnitude of 0·592 mm for the HEAVYPIS case.

In this example, the proposed analytical methodology for calculating the dynamic behavior of engine crankshafts clearly predicted the experimentally observed vibratory behavior of the crankshaft–flywheel assembly (see Figure 18) and correctly indicated the dominant third order resonance around 4800 r.p.m. and the high DC (mean) value of the flywheel axial vibratory displacement. It also showed analytically that internal balancing of the crankshaft with simultaneous reduction of the flywheel mass could eliminate the problem of high vibration levels at the rear bearing cap. This finding was subsequently validated experimentally.

7. SUMMARY AND CONCLUSIONS

This paper describes a structural analysis using dynamic substructuring with Ritz vectors for predicting the dynamic response of an engine crankshaft, based on the finite-element method. A two-level dynamic substructuring is used. Initially, a given three-dimensional

finite-element model of the crankshaft is divided into substructures. Each substructure is dynamically reduced using a set of load-dependent Ritz vectors. Subsequently, all substructures are assembled and a second dynamic reduction is performed using a new set of Ritz vectors. A subspace algorithm is used to generate the load-dependent Ritz vectors. The algorithm is implemented in MSC/NASTRAN using developed DMAP ALTERS in order to utilize the excellent data management capabilities of MSC/NASTRAN. After the two dynamic reductions, the reduced model is integrated in time using Newmark's method.

In the model, the rotating crankshaft is properly coupled with the non-rotating, compliant engine block. The block compliance is represented by a distributed linear elastic foundation at each main bearing location. The stiffness of the elastic foundation can be different in the vertical and horizontal planes, thereby considering the anisotropy of the engine block compliance with respect to the crankshaft rotation. The analysis accounts for the kinematic non-linearity resulting from the crankangle-dependent circumferential contact location between each journal and the corresponding bore of the engine block. Crankshaft "bent" and block "misboring" effects, due to manufacturing imperfections, are also considered in the analysis.

The accuracy and efficiency of the developed method was demonstrated by comparison with the equivalent superelement analysis in MSC/NASTRAN. Free and forced vibrations of a slender cylindrical beam and free vibrations of a four-cylinder engine crankshaft were examined. In all cases, the present method gave superior accuracy with less computational effort compared with MSC/NASTRAN. Furthermore, the accuracy of the present method is illustrated through comparisons with experimental results for the torsional vibrations of an in-line five-cylinder engine and the bending vibrations of the crankshaft-flywheel assembly of a V6 engine.

The present analysis can be used to predict the crankshaft dynamic response, main bearing loads and dynamic stresses throughout the engine cycle. The effect of a wide variety of design variables can be studied. Such variables include, among others, counterweights, reciprocating and rotating masses, crankshaft geometry, crankshaft "bent" and engine block "misboring", lower block design (bulkhead and bearing cap stiffness, mounting positions), flywheel design (dimensions, material) and belt loads. The presented structural analysis can be also coupled with the main bearing hydrodynamics in a crankshaft-main bearing-engine block system model. Such a model can predict the main bearing loads very accurately resulting in better assessment of (1) main bearing performance and (2) engine block radiated noise due to main bearing load excitation.

ACKNOWLEDGMENTS

The author wishes to express his gratitude to Dr Turgay Bengisu from the Synthesis and Analysis Department of the General Motors Powertrain Division for providing access to the experimental results presented in this paper. Furthermore, his efforts in developing, productionizing and institutionalizing CRANKSYM within General Motors are greatly appreciated. His knowledge and experience on engine crankshaft vibrations and on vibrations in general have been invaluable in developing and improving CRANKSYM over the past few years.

REFERENCES

1. G. W. GREEN 1987 *Society of Automotive Engineers*, *Paper* 870579. Design of crankshafts by the finite element method.

2. A. R. HEATH and P. M. MCNAMARA 1989 *Engine Design Operation and Control Using Computer Systems*, *ASME-ICE*, Vol. 9. Crankshaft stress analysis—the combination of finite element and classical analysis techniques.
3. P. M. MCNAMARA and J. TREVELYAN 1991 *Proceedings of the International Conference on Computers in Engine Technology*, *Institute of Mechanical Engineers*. Crankshaft stress analysis—the combination of finite element and boundary element techniques.
4. H. OKAMURA, A. SHINNO, T. YAMANAKA, A. SUZUKI and K. SOGABE 1990 *ASME Winter Annual Meeting—Vehicle Noise*, 47–58. A dynamic stiffness matrix approach to the analysis of three-dimensional vibrations of automobile engine crankshafts: Part 1—background and application to free vibrations.
5. T. MORITA and H. OKAMURA 1990 *ASME Winter Annual Meeting—Vehicle Noise*, 59–66. A dynamic stiffness matrix approach to the analysis of three-dimensional vibrations of automobile engine crankshafts: Part 2—application to firing conditions.
6. B. LAW and I. T. MARTIN 1989 *Institute of Mechanical Engineers*, *Paper* C382/046, 487–498. Prediction of crankshaft and flywheel dynamics.
7. H. KATANO, A. IWAMOTO and T. SAITOH 1991 *Institute of Mechanical Engineers*, *Paper* C430/049, 205–216. Dynamic behaviour analysis of internal combustion engine crankshafts under operating conditions.
8. M. KUBOTA, R. KAMICHIKA, K. TANIDA and E. NAKAGAWA 1988 *Bulletin of the Marine Engineering Society in Japan*, Vol. 16, No. 2. Dynamic analysis of crankshaft using component mode synthesis: Part 1—efficient method of calculations utilizing NASTRAN image superelements.
9. K. TANIDA, M. KUBOTA N. HASEGAWA and E. NAKAGAWA 1988 *Bulletin of the Marine Engineering Society in Japan*, Vol. 16, No. 2. Dynamic analysis of crankshaft using component mode synthesis: Part 2—application to long stroke diesel engine.
10. O. KURODA and Y. FUJII 1988 *Society of Automotive Engineers*, *Paper* 880083. Approach to improve engine sound quality.
11. J. AFFENZELLER and G. E. THIEN 1982 *Society of Automotive Engineers*, *Paper* 820435. Evaluating engine design for low noise using dynamic structural modeling.
12. J. AFFENZELLER, H. H. PRIEBSCH and G. KUIPERS 1990 *Society of Automotive Engineers*, *Paper* 900019. Structure borne noise prediction techniques.
13. H. H. PRIEBSCH, J. AFFENZELLER and S. GRAN 1991 CIMAC, Paper D59. Prediction techniques for vibration and stress of nonlinear supported rotating crankshafts.
14. M. A. GOCKEL (editor) 1982 *The McNeal–Schwendler Corp. MSC/NASTRAN*: *Handbook for Superelement Analysis*.
15. R. R. CRAIG JR. 1981 *Structural Dynamics—An Introduction to Computer Methods*. New York, NY: John Wiley & Sons.
16. M. A. GOCKEL (editor) 1983 *The McNeal–Schwendler Corp. MSC/NASTRAN*: *Handbook for Dynamic Analysis*.
17. E. L. WILSON M. W. YUAN and J. M. DICKENS 1982 *Earthquake Engineering and Structural Dynamics* **10**, 813–821. Dynamic analysis by direct superposition of Ritz vectors.
18. E. BAYO and E. L. WILSON 1984 *Earthquake Engineering and Structural Dynamics* **12**, 499–505. Use of Ritz vectors in wave propagation and foundation responses.
19. R. R. ARNOLD, R. L. CITERLEY, M. CHARGIN and D. GALANT 1985 *Computers and Structures* **21**, 461–467. Application of Ritz vectors for dynamic analysis of large structures.
20. E. L. WILSON and E. P. BAYO 1986 *Journal of Structural Engineering* **112**, 1944–1954. Use of special Ritz vectors in dynamic substructure analysis.
21. P. LEGER and E. L. WILSON 1987 *Engineering Computations* **4**, 309–318. Generation of load dependent Ritz transformation vectors in structural dynamics.
22. K. J. JOO and E. L. WILSON 1989 *Earthquake Engineering and Structural Dynamics* **18**, 149–167. Ritz vectors and generation criteria for mode superposition analysis.
23. S. R. IDELSON and A. CARDONA 1985 *Computer Methods in Applied Mechanics and Engineering* **49**, 253–279. A load dependent basis for reduced nonlinear structural dynamics.
24. R. J. GUYAN 1965 *AIAA Journal* **3**, 380. Reduction of stiffness and mass matrices.
25. P. LEGER 1988 *Computers and Structures* **29**, 993–999. Load dependent subspace reduction methods for structural dynamic computations.
26. L. KMZSIK (editor) 1990 *The McNeal–Schwendler Corp. MSC/NASTRAN*: *Handbook for Numerical Methods*.
27. R. R. CRAIG and M. C. C. BAMPTON 1968 *AIAA Journal* **6**, 1313–1319. Coupling of substructures for dynamic analysis.

28. M. A. REYMOND (editor) 1991 *The McNeal–Schwendler Corp. MSC/NASTRAN: User's Manual.*
29. K. J. BATHE and E. L. WILSON 1976 *Numerical Methods in Finite Element Analysis.* Englewood Cliffs, NJ: Prentice-Hall, Inc.
30. E. VON SCHNURBEIN 1970 *Transactions of the Society of Automotive Engineers, Paper* 700716. A new method of calculating plain bearings of statically indeterminate crankshafts.
31. N. M. NEWMARK 1959 *Proceedings of the American Society of Civil Engineers.* A method of computation for structural dynamics.

APPENDIX A. A SUBSPACE ALGORITHM TO CALCULATE LOAD-DEPENDENT RITZ VECTORS

1. *Given input matrices*
   $[M]$: mass matrix $(n \times n)$
   $[K]$: stiffness matrix $(n \times n)$
   $[F]$: block of k independent spatial load vectors $(n \times k)$
2. T*riangularize stiffness matrix*

   $$[K] = [L]^{\mathrm{T}}[D][L]$$

3. *Solve for initial static block* $[X_1]$
   (a) Solve for block $[x^*] = [x_1^*, x_2^*, \ldots, x_k^*]$,

   $$[K][x^*] = [F].$$

   (b) Get block $[\bar{X}] = [\bar{x}_1, \bar{x}_2, \ldots, \bar{x}_k]$ by M-normalization of vectors $\{x_j^*\}$, $j = 1, 2, \ldots, k$: $\{x_j^*\}^{\mathrm{T}}[M]\{x_j^*\} = a$, $\{\bar{x}_j\} = a^{-1/2}\{x_j^*\}$.
   (c) Get block $[\hat{X}] = [\hat{x}_1, \hat{x}_2, \ldots, \hat{x}_k]$ by M-orthogonalization of vectors in $[\bar{X}]$. Repeat for $j = 2, 3, \ldots, k$:

   $$[C_j] = [\bar{x}_1, \bar{x}_2, \ldots, \bar{x}_{j-1}]^{\mathrm{T}}[M]\{\bar{x}_j\}, \quad \{\hat{x}_j\} = \{\bar{x}_j\} - [\bar{x}_1, \bar{x}_2, \ldots, \bar{x}_{j-1}][C_j].$$

   (d) M-normalize block $[\hat{X}]$: $[\hat{X}]^{\mathrm{T}}[M][\hat{X}] = [\Lambda]$, $[X_1] = [\hat{X}][\Lambda]^{-1/2}$.
4. *Solve for subsequent blocks* $[X_i]$, $i = 2, 3, \ldots, p$
   (a) Solve for block $[X_i^*]$: $[K][X_i^*] = [M][X_{i-1}]$.
   (b) Get block $[\hat{X}_i]$ by M-orthogonalization of $[X_i^*]$ against all previous blocks:

   $$[C] = [[X_1], \ldots, [X_{i-1}]]^{\mathrm{T}}[M][X_i^*],$$
   $$[\hat{X}_i] = [X_i^*] - [[X_1], \ldots, [X_{i-1}]][C].$$

   (c) Get block $[\bar{X}_i]$ by M-orthogonalization of $[\hat{X}_i]$ against all previous blocks according to step 4b.
   (d) Get block $[X_i]$ by M-orthogonalization of block $[\bar{X}_i]$ according to steps 3c and d.

APPENDIX B: NOMENCLATURE

$[C]$	damping matrix
$f(s)$	space function
$\{F\}$	load vector
$g(t)$	time function
$[I]$	identity matrix
k	translational engine block stiffness at main bearing locations
$[K]$	stiffness matrix
$[M]$	mass matrix
s	space
t	time

$[T]$ static transformation matrix
$\{u\}$ generalized displacement vector
$\{U\}$ displacement vector
$\{U_i\}$ internal displacement vector
$\{U_r\}$ retained displacement vector
$\{U_o^c\}$ vector representing the crankshaft "bent"
$\{U_o^b\}$ vector representing the engine block "misboring"
(x, y, z) right-handed rotating coordinate system
(X, Y, Z) right-handed fixed coordinate system
$[X]$ transformation basis matrix

Greek symbols
α, β constants to describe Rayleigh damping
$\{\varepsilon\}$ bearing eccentricity vector
ζ damping ratio
θ crankangle
$[\phi]$ total transformation matrix
ω rotational speed or natural frequency

Subscripts
i internal quantities (displacement, stiffness, mass, etc.)
o offset
r retained quantities (displacement, stiffness, mass, etc.)
T total displacement
x, y vertical and horizontal directions, respectively, in rotating coordinate system
X, Y vertical and horizontal directions, respectively, in fixed coordinate system
1, 2 levels of substructuring

Superscripts
b engine block
c crankshaft
T transpose
ℓ substructure number
1, 2, 3, … substructure number

Miscellaneous
– reduced matrix or vector
$\cdot$ single time differentiation
$\cdot\cdot$ double time differentiation